Increased electrical conductivity in fine-grained (Zr,Hf)NiSn based thermoelectric materials with nanoscale precipitates

Han-Hui Xie,[1] Cui Yu,[1] Tie-Jun Zhu,[1,2,a)] Chen-Guang Fu,[1] G. Jeffrey Snyder,[3] and Xin-Bing Zhao[1]
[1]*State Key Laboratory of Silicon Materials and Department of Materials Science and Engineering, Zhejiang University, Hangzhou 310027, China*
[2]*Cyrus Tang Center for Sensor Materials and Applications, Zhejiang University, Hangzhou 310027, China*
[3]*Materials Science, California Institute of Technology, Pasadena, California 91125, USA*

(Received 19 March 2012; accepted 7 June 2012; published online 21 June 2012)

Grain refinement has been conducted to reduce the thermal conductivity and improve the thermoelectric performance of the (Zr,Hf)NiSn based half-Heusler alloys. Nanoscale *in situ* precipitates were found embedded in the matrix with submicron grains. The lattice thermal conductivity was decreased due to the enhanced boundary scattering of phonons. The increased carrier concentration and electrical conductivity were observed compared to the coarse-grained alloys, which is discussed in relation to the existence of nanoscale precipitates, the effect of antisite defects, and composition change. It is suggested that the nanoscale precipitates play a significant role in the observed electrical conductivity increase. © *2012 American Institute of Physics*. [http://dx.doi.org/10.1063/1.4730436]

In past decades, thermoelectric (TE) materials have received rejuvenated interest due to their promising applications in direct thermal to electric energy conversion and solid-state refrigeration. The performance of a TE material is represented by the dimensionless figure of merit $ZT=\alpha^2\sigma T/\kappa$, where α is the Seebeck coefficient, σ is the electrical conductivity, κ is the thermal conductivity mainly including the electron contribution κ_e and the lattice contribution κ_L, and T is the absolute temperature.[1,2]

The *M*NiSn-based (M = Zr, Hf, and Ti) half-Heusler compounds have recently been identified as potential high temperature TE materials for power generation up to 1100 K.[3–5] Their combination of high Seebeck coefficients and moderate electrical conductivities gives rise to intrinsically high TE power factors.[6,7] However, the high thermal conductivity ($\kappa \approx 10\,\mathrm{Wm^{-1}K^{-1}}$) makes this system less promising for TE applications.[7] Several strategies for suppressing the lattice thermal conductivity by increasing phonon scattering via point defects or grain boundary scattering have been implemented.[4–10] High ZT values of >0.8 have been achieved in the Sb doped (Zr,Hf)NiSn based alloys.[5,10]

Although boundary scattering is generally effective in suppressing the lattice thermal conductivity, the reduction of grain sizes will also induce a decrease in electrical conductivity due to the enhanced scattering for both electrons and phonons. Sharp *et al.* proposed that for the *M*NiSn alloys, the lattice thermal conductivity would decrease faster than the carrier mobility below tens of micrometers of grain sizes, because the mean free path of phonons is larger than that of electrons in the alloys.[11] In this work, the *M*NiSn based alloys with submicron grain sizes were prepared by melt spinning in order to enhance the phonon scattering and keep the electrical properties almost unchanged. Unexpectedly, an electrical conductivity increase was observed, although the lattice thermal conductivity was decreased to some extent due to the reduced grain sizes. Possible causes are discussed and it is suggested that the nanoscale *in situ* precipitates in the matrix play a significant role in the electrical conductivity increase.

The ingots of $Hf_{1-x}Zr_xNiSn_{1-y}Sb_y$ ($0 \le x \le 1$ and $0 \le y \le 0.02$) were prepared by levitation melting.[10] Part of the ingot was inductively re-melted and injected onto the edge of a rotating copper roller with a linear speed of 45 m/s.[12] The melt spun (MS) thin ribbons and the remained levitation melted (LM) ingots were, respectively, pulverized and sintered by spark plasma sintering (SPS) at 1103 K for 15 min under 65 MPa. The densities of all the samples are ~95% of theoretical ones.

The powder x-ray diffraction analysis showed that all samples were single phase. The electrical conductivity was measured on a computer-aided system using a DC four-probe method. The thermal conductivity κ was calculated by $\kappa = D\rho_D C_p$, where ρ_D is the sample density. The thermal diffusivity D and specific heat C_p above room temperature were measured on a Netzsch LFA457 laser flash apparatus. The carrier concentration was measured on a Quantum Design PPMS-9T system.

Figure 1 shows the temperature dependence of lattice thermal conductivity for the $Hf_{1-x}Zr_xNiSn_{1-y}Sb_y$ ($0 \le x \le 1$ and $0 \le y \le 0.02$) samples. The lattice thermal conductivity κ_L was derived by subtracting electronic component κ_e from total thermal conductivity κ. The κ_e was estimated using the Wiedemann-Franz law $\kappa_e = L_0\sigma T$ with the Lorenz number L_0 of $2.0 \times 10^{-8}\ \mathrm{W \cdot \Omega \cdot K^{-2}}$ for a degenerate semiconductor.[10] As expected, the κ_L of the fine-grained MS samples is decreased, compared with the coarse-grained LM counterparts, due to the enhanced phonon boundary scattering. The Zr substituted alloys have lower κ_L than the end compositions owing to the mass fluctuation scattering. The κ_L decreases with temperature for all samples, but still much higher than the minimum thermal conductivity κ_{min} calculated by Cahill's model.[13]

a)Corresponding author. Electronic mail: zhutj@zju.edu.cn.

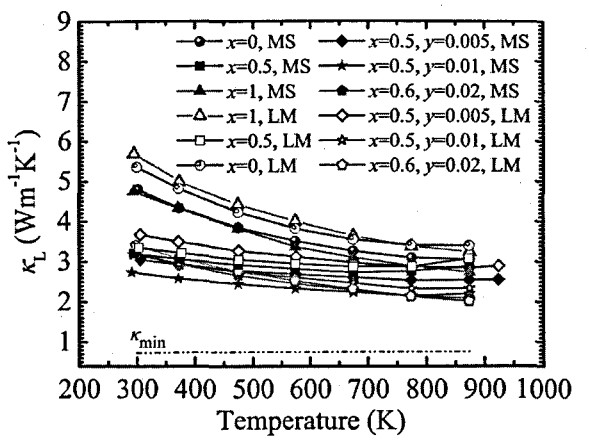

FIG. 1. Lattice thermal conductivity κ_L for the MS and LM $Hf_{1-x}Zr_xNiSn_{1-y}Sb_y$ samples with and without Sb doping. The dash line represents the calculated minimum thermal conductivity κ_{min} of the $Hf_{0.4}Zr_{0.6}NiSn_{0.98}Sb_{0.02}$ alloy.

Figure 2 shows the electrical conductivity for the $Hf_{1-x}Zr_xNiSn_{1-y}Sb_y$ ($0 \le x \le 1$ and $0 \le y \le 0.02$) samples. Surprisingly, despite smaller grain sizes, the MS sample of each composition exhibits higher electrical conductivity compared to the LM counterpart. Table I lists the room temperature physical properties of some samples, indicating that the MS samples also have higher carrier concentrations and lower Seebeck coefficients, which is consistent with

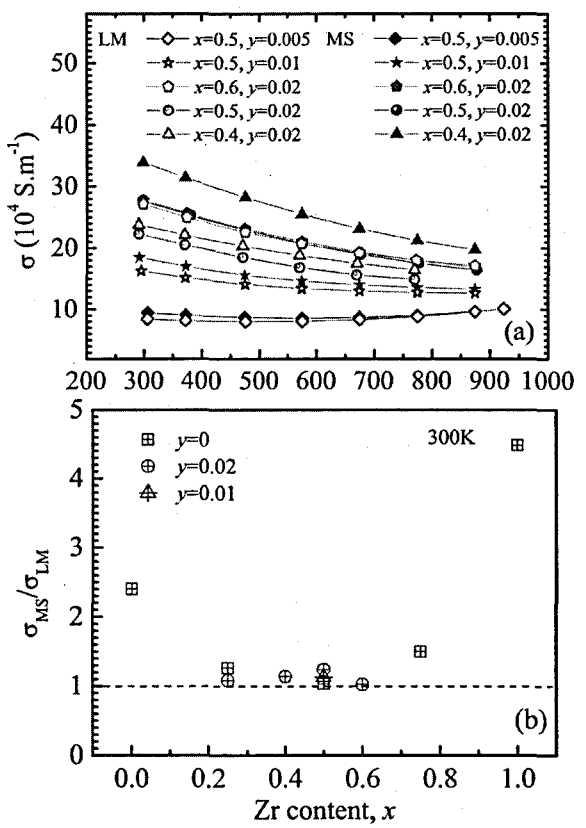

FIG. 2. Temperature dependence of electrical conductivity for the $Hf_{1-x}Zr_xNiSn_{1-y}Sb_y$ alloys (a), and the electrical conductivity ratio of the MS and LM samples at room temperature as a function of Zr content (b).

TABLE I. Carrier concentration n_H, electrical conductivity σ, and Seebeck coefficient α of the LM and MS $Hf_{1-x}Zr_xNiSn_{1-y}Sb_y$ alloys at room temperature.

Composition	Preparation	σ ($10^4 S \cdot m^{-1}$)	n_H ($10^{25} m^{-3}$)	α ($\mu V \cdot K^{-1}$)
HfNiSn	LM	1.03	5	−178.0
	MS	2.39	13	−128.5
$Hf_{0.75}Zr_{0.25}NiSn$	LM	1.63	19	−107.5
	MS	2.06	20	−106.4
$Hf_{0.5}Zr_{0.5}NiSn_{0.99}Sb_{0.01}$	LM	16.29	36	−121.3
	MS	18.48	45	−101.3
$Hf_{0.5}Zr_{0.5}NiSn_{0.98}Sb_{0.02}$	LM	22.3	52.4	−100.8
	MS	27.59	102	−86.1
$Hf_{0.6}Zr_{0.4}NiSn_{0.98}Sb_{0.02}$	LM	29.67	100	−102.2
	MS	33.92	132	−80.4

our previous results.[12] Three possible causes may account for the electrical conductivity increase in the MS samples: the composition change, antisite defects, or phase separation, which will be discussed in the following paragraph.

The real compositions of all samples were detected by electron probe microanalysis (EPMA) with wavelength dispersive spectrometer. The composition of the MS samples and the LM counterparts displayed no obvious distinction, taking consideration of the measurement errors. Given that the resolution for EPMA is approximately 0.2% atomic accuracy and such a change in composition of any element could result in $\sim 10^{25}$ carriers/m^{-3} (assuming 1 electron per compositional defect), the observed carrier concentration difference due to composition may be beyond the resolution of EPMA. However, the composition fluctuation alone cannot explicitly explain why the electrical conductivities of all MS samples are always higher than those of the LM counterparts [Fig. 2(b)].

It is generally accepted that there exist Zr/Sn antisite defects in ZrNiSn based alloys due to the similar atom sizes of Zr and Sn. Remarkable electrical conductivity decrease by a factor of ~100% has been observed at room temperature in arc-melted ZrNiSn samples with prolonged annealing duration, which was attributed to the reduction in the content of Zr/Sn antisite defects.[7,14] Theoretical calculation shows that the band gap decreases with increasing antisite disorder content that could result in increased electrical conductivity.[14] It is possible that the rapid solidification by melt spinning induced increased Zr/Sn antisite defects. Therefore, several samples were annealed at 800 °C for 5 days to check for the effect of such antisite defects. However, as shown in Fig. 3, no noticeable change was observed in the electrical conductivity before and after annealing of the same compositions for the undoped samples, suggesting that the concentrations of antisite defects in both MS and LM samples are negligible. The discrepancy between the previous report (Ref. 14) and this work may result from the different fabrication processing and phase purity. The recent Rietveld refinements based on high-resolution synchrotron radiation x-ray diffraction of our single phase LM samples also do not indicate the existence of Zr/Sn antisite disorder.[15]

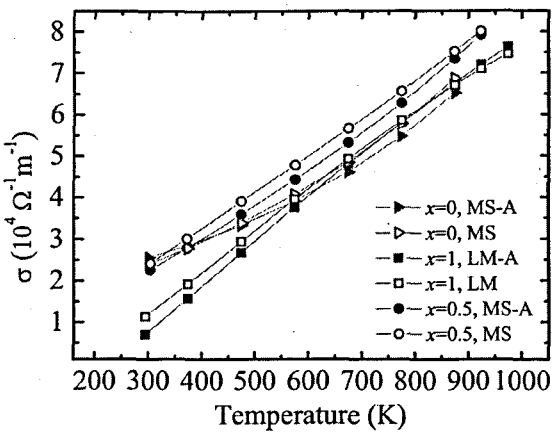

FIG. 3. Temperature dependence of electrical conductivity for undoped LM and MS $Hf_{1-x}Zr_xNiSn$ samples before and after annealing at 800 °C for 5 days. Here, "A" means annealing.

Finally, transmission electron microscopy (TEM) observation was performed to further investigate the microstructure of samples. The scanning electron microscopy observation in our previous work has shown that there exist nanoscale particles on the free surfaces of melt spun ribbons.[16] Figure 4 shows the typical TEM images for the $Hf_{0.6}Zr_{0.4}NiSn_{0.98}Sb_{0.02}$ bulk sample by melt spinning followed by SPS, the grain sizes of which are of submicron scale with many *in-situ* nanoparticles embedded in the matrix. Such a nanostructure was not observed in the LM samples. The similar TEM images were also found in the ZiNiSn based alloys with excess Ni,[17] and the nanoparticles were suggested to be metal Ni-rich Heulser phases. However, the inter-plane distance of the nanophase (3.9 Å) here cannot be indexed to any crystal plane of the HH or Heusler phase in this work.

It has been suggested that metallic/semimetallic nanoinclusions inside a semiconductor host can contribute conduction electrons to the matrix and hence increase electrical conductivity.[18–20] It can be expected that the size, spacing, and shape of the nanophases affect the position of the Fermi level and the conduction electron concentration of the matrix.[19] Although the exact compositions of the small precipitates could not be confirmed at this stage, these nanoscale phases may be more metallic than the matrix, resulting in increased carrier concentration and electrical conductivity in the MS samples. It is also possible that these nanoscale phases induce defects and local composition fluctuation that introduce carriers into the matrix. However, it cannot be conclusively determined how much these nanoparticles affect the observed carrier concentrations. In addition, the presence of nanophases is also favorable to the reduction in the lattice thermal conductivity or the increase in the Seebeck coefficient of thermoelectric materials.[21–23]

The figure of merit of all samples was calculated and a maximum *ZT* of 0.9 was achieved at 973 K for the melt-spun $Hf_{0.6}Zr_{0.4}NiSn_{0.98}Sb_{0.02}$ sample,[12] comparable with that of the levitation melted coarse-grained counterpart.[10] Therefore, despite the simultaneous electrical conductivity increase and lattice thermal conductivity reduction, no significant enhancement in *ZT* was obtained for the MS alloys

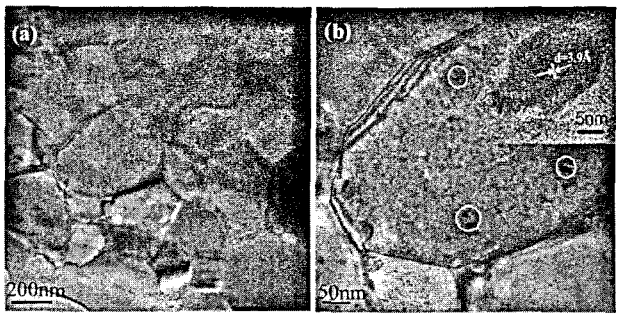

FIG. 4. TEM images of the MS $Hf_{0.6}Zr_{0.4}NiSn_{0.98}Sb_{0.02}$ bulk sample, showing the submicron grains (a) and embedded *in-situ* nanophases (b). The inset in (b) is the high resolution TEM image of a nanophase.

with the submicron matrix and embedded nanophases due to the concomitantly decreased Seebeck coefficient and increased electronic thermal conductivity.

In summary, fine-grained (Zr,Hf)NiSn based half-Heusler thermoelectric materials have been fabricated. The electrical conductivity increase was observed compared to the coarse-grained counterparts, although the lattice thermal conductivity was decreased due to the enhanced boundary scattering of phonons. This may be associated with the existence of metallic nano-precipitates embedded in the matrix.

We acknowledge the use of EPMA in the Key Laboratory of Submarine Geosciences, State Oceanic Administration, China. T.J.Z. would like to thank Dr. Yanzhong Pei and Heng Wang from California Institute of Technology for the valuable discussions. The work is supported by the Natural Science Foundation of China (51171171, 51061120455, and 50971115) and the Fundamental Research Funds for the Central Universities (2011QNA4034).

[1]T. M. Tritt, Science **283**, 804 (1996).
[2]G. J. Snyder and E. S. Toberer, Nature Mater. **7**, 105 (2008).
[3]H. Hohl, A. P. Ramirez, C. Goldmann, G. Ernst, B. Woelfing, and E. Bucher, J. Phys.: Condens. Matter. **11**, 1697 (1999).
[4]G. Joshi, X. Yan, H. Wang, W. Liu, G. Chen, and Z. Ren, Adv. Energy Mater. **1**, 643 (2011).
[5]S. R. Culp, S. J. Poon, N. Hickman, T. M. Tritt, and J. Blumm, Appl. Phys. Lett. **88**, 042106 (2006).
[6]Q. Shen, L. Chen, T. Goto, T. Hirai, J. Yang, G. P. Meisner, and C. Uher, Appl. Phys. Lett. **79**, 4165 (2001).
[7]C. Uher, J. Yang, S. Hu, D. T. Morelli, and G. P. Meisner, Phys. Rev. B **59**, 8615 (1999).
[8]S. Bhattacharya, T. M. Tritt, Y. Xia, V. Ponnambalam, S. J. Poon, and N. Thadhani, Appl. Phys. Lett. **81**, 43 (2002).
[9]S. Bhattacharya, M. J. Skove, M. Russell, T. M. Tritt, Y. Xia, V. Ponnambalam, S. J. Poon, and N. Thadhani, Phys. Rev. B **77**, 184203 (2008).
[10]C. Yu, T. J. Zhu, R. Z. Shi, Y. Zhang, X. B. Zhao, and J. He, Acta Mater. **57**, 2757 (2009).
[11]J. W. Sharp, S. J. Poon, and H. J. Goldsmid, Phys. Status Solidi A **187**, 507 (2001).
[12]C. Yu, T. J. Zhu, K. Xiao, J. J. Shen, S. H. Yang, and X. B. Zhao, J. Electr. Mater. **39**, 2008 (2010).
[13]D. G. Cahill, S. K. Watson, and R. O. Pohl, Phys. Rev. B **46**, 6131 (1992).
[14]P. F. Qiu, J. Yang, X. Y. Huang, X. H. Chen, and L. D. Chen, Appl. Phys. Lett. **96**, 152105 (2010).
[15]H. H. Xie, J. L. Mi, L. P. Hu, N. Lock, M. Chirstensen, C. G. Fu, B. B. Iversen, X. B. Zhao, and T. J. Zhu, Cryst. Eng. Commun. **14**, 4467 (2012).
[16]C. Yu, T. J. Zu, K. Xiao, J. J. Shen, and X. B. Zhao, Funct. Mater. Lett. **3**, 227 (2010).
[17]J. P. A. Makongo, D. K. Misra, X. Zhou, A. Pant, M. R. Shabetai, X. Su, C. Uher, K. L. Stokes, and P. F. P. Poudeu, J. Am. Chem. Soc. **133**, 18843 (2011).

[18]J. M. Zide, D. O. Klenov, S. Stemmer, A. C. Gossard, G. Zeng, J. E. Bowers, D. Vashaee, and A. Shakouri, Appl. Phys. Lett. **87**, 112102 (2005).
[19]D. C. Driscoll, M. Hanson, C. Kadow, and A. C. Gossard, Appl. Phys. Lett. **78**,1703 (2001).
[20]J. P. Heremans, C. M. Thrush, and D. T. Morelli, J. Appl. Phys. **98**, 063703 (2005).
[21]S. Johnsen, J. Q. He, J. Androulakis, V. P. Dravid, I. Todorov, D. Y. Chung, and M. G. Kanatzidis, J. Am. Chem. Soc. **133**, 3460 (2011).
[22]J. Q. He, J. R. Sootsman, L. Q. Xu, S. N. Girard, J. C. Zheng, M. G. Kanatzidis, and V. P. Dravid, J. Am. Chem. Soc. **133**, 8786 (2011).
[23]K. Biswas, J. Q. He, Q. C. Zhang, G. Y. Wang, C. Uher, V. P. Dravid, and M. G. Kanatzidis, Nat. Chem. **3**, 160 (2011).